Materials Advances

ROYAL SOCIETY OF CHEMISTRY

PAPER

View Article Online
View Journal | View Issue

Cite this: *Mater. Adv.*, 2025, **6**, 9196

Deposition time-driven growth of gold nanoparticles for enhanced performance in ethanol electrooxidation

Setia Budi, *[a] Annisa Auliya[a] and Hilman Syafei[b]

Received 17th July 2025,
Accepted 19th October 2025

DOI: 10.1039/d5ma00768b

rsc.li/materials-advances

Gold nanoparticles (AuNPs) exhibit unique catalytic, electronic, and optical properties, making them highly suitable for various applications, particularly in catalysis. This study explores the synthesis of AuNPs on fluorine-doped tin oxide substrates using a square-wave pulse deposition technique, with deposition time as the primary variable influencing nanoparticles growth. The synthesized AuNPs were systematically characterized using field emission scanning electron microscopy, energy dispersive X-ray spectroscopy, and X-ray diffraction techniques. The electrocatalytic performance of the synthesized AuNPs was evaluated through electrochemical impedance spectroscopy and cyclic voltammetry in an alkaline medium. The results revealed that longer deposition duration led to nanoparticle increased coverage, improved charge transfer kinetics, and enhanced catalytic activity. Notably, AuNPs50 deposited for 50 minutes exhibited the the lowest charge transfer resistance and the highest electrochemical surface area, resulting in the highest current density during ethanol electrooxidation. These findings demonstrate the enhanced catalytic performance of the electrodeposited AuNPs for ethanol oxidation, achieved without the use of surfactants or additives.

1 Introduction

Gold nanoparticles (AuNPs) have attracted considerable scholarly interest owing to their distinctive optical, electronic, and chemical properties. These characteristics make AuNPs highly valuable for a diverse array of applications, including electronics,[1] biomedicine,[2] sensing,[3,4] and catalysis.[5] In the field of catalysis, the performance of AuNPs is strongly influenced by their morphology and particle size. This dependency has driven the development of various synthesis techniques aimed at controlling these parameters.[6–10] A notably advantageous characteristic of nanosized-gold particles catalysts is the high density of active sites, which can significantly enhance catalytic activity.[11–13] As a non-platinum catalyst, gold has demonstrated promising catalytic activity for the electrooxidation of ethanol in alkaline media, with performance that is comparable to or even superior to platinum-based catalysts.[14] Furthermore, the adsorption of hydroxide anion (OH^-) at lower potentials, combined with the reduced susceptibility to poisoning by carbon monoxide intermediates, contributes to the enhanced efficiency of AuNP-based catalysts in ethanol electrooxidation reactions.[15]

Contemporary approaches for the synthesizing AuNPs with controlled morphologies often involve the use of additives,[16] surfactants,[17] or templates.[18] However, surfactants and directing agents can introduce impurities, while template-assisted methods typically require post-synthetic treatments that may compromise the structural integrity of the nanomaterials.[19,20] In contrast, electrodeposition offers a rapid, straightforward,[21] and effective approach for synthesizing nanomaterials with well-defined structures,[22,23] without the need for additives, surfactants, or templates.[24,25] Key parameters in the electrodeposition process, such as applied voltage, pH, electrolyte concentration, and deposition duration, can be systematically adjusted to influence surface coverage, particle morphology, and size.[26–28] These structural characteristics play a critical role in determining the electrocatalytic performance of AuNPs.

In this study, the square-wave pulse deposition technique was employed due to its ability to precisely control the deposition process, specifically nucleation and growth, by alternating between two distinct potentials over a defined time interval. This approach is essential for producing controlled-size nanoparticles from an additive-free solution, which can significantly influence the performance of the ethanol electrooxidation reaction (EOR). The deposition time was used as the primary parameter to regulate AuNPs *via* this technique. By minimizing excessive growth, the method aims to preserve the catalytic activity of the nanoparticles. The synthesized AuNPs were

[a] *Department of Chemistry, Faculty of Mathematics and Natural Sciences, Universitas Negeri Jakarta, Jl. Rawamangun Muka, Jakarta 13220, Indonesia. E-mail: setiabudi@unj.ac.id*
[b] *The Center for Science Innovation, Arva Building, Jl. RP. Soeroso, Jakarta Pusat 10350, Indonesia*

subsequently evaluated for their catalytic performance in ethanol oxidation in alkaline solutions.

2 Materials and methods

2.1 Materials

Chloroauric acid ($HAuCl_4 \cdot 3H_2O$), used as the precursor for gold nanoparticles (AuNPs) synthesis, was obtained from Sigma-Aldrich. Additional chemicals, including sulfuric acid (H_2SO_4), ethanol (C_2H_5OH, 96%), sodium hydroxide (NaOH), and potassium chloride (KCl), were purchased from Merck. All reagents were dissolved in deionized water. Fluorine-doped tin oxide (FTO) coated glass, with a sheet resistance of 10 Ω sq^{-1}, was used as the substrate nanoparticles deposition.

2.2 Synthesis of gold nanoparticles

AuNPs were synthesized on FTO substrates *via* electrodeposition using an electrolyte solution containing 0.5 mM $HAuCl_4 \cdot 3H_2O$ and 0.5 M H_2SO_4. The deposition was carried out at room temperature using a square-wave pulse deposition technique. The applied upper and lower potentials were set at 0.0 V and −0.1 V *versus* an Ag/AgCl reference electrode, as illustrated in Fig. 1. The electrodeposition was performed using an ER466 potentiostat configured for a three-electrode system. A platinum plate (8 × 7 mm^2) served as the counter electrode, while the Ag/AgCl (3 M KCl) acted as reference electrode. The FTO substrate (3 × 10 mm^2) functioned as the working electrode. The deposition time was systematically varied between 1 and 50 minutes, resulting in samples labeled AuNPs1, AuNPs5, AuNPs10, and AuNPs50, corresponding to their respective deposition durations.

2.3 Characterization of morphology and structure

The morphology of the deposited AuNPs was examined using field emission scanning electron microscopy (FESEM, Thermo Scientific Quattro S). The elemental composition analysis was carried out *via* energy dispersive X-ray spectroscopy (EDX). Structural characterization of the samples was performed using X-ray diffraction technique (XRD, Bruker D8 Advance).

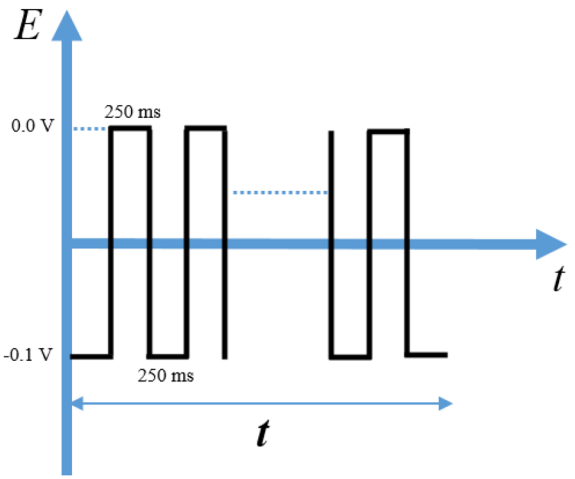

Fig. 1 Electrodeposition schematic of the AuNPs using square-wave pulse deposition conducted by varying deposition duration.

2.4 Electrochemical analysis

The electrochemical properties of the AuNPs were investigated using electrochemical impedance spectroscopy (EIS) technique using a CorrTest CS310 electrochemical workstation, conducted in a 0.5 M KCl solution. The EIS measurements were conducted in a three-electrode configuration comprising an Ag/AgCl (3 M KCl) reference electrode, a platinum as the counter electrode, and the gold-deposited fluorine-doped tin oxide (FTO) substrate as the working electrode. The frequency range employed for EIS analysis was set between 0 and 50 kHz.

The electrocatalytic activity of AuNPs toward ethanol oxidation of ethanol was evaluated using cyclic voltammetry (CV) technique within a potential range of −0.75 to 0.75 V at a scan rate of 25 mV s^{-1}. The measurements were performed using an ER466 potentiostat in an electrolyte solution containing 1 M ethanol and 0.1 M NaOH.

3 Results and discussion

The morphology of gold nanoparticles (AuNPs) synthesized on fluorine-doped tin oxide (FTO) substrates at varying deposition times was examined through the application of field emission scanning electron microscopy (FESEM). As shown in Fig. 2, the AuNPs deposited for a duration of one minute (denoted as AuNPs1) exhibit irregular spherical shapes with relatively sparse distribution across the substrate surface. With increasing deposition durations of 5 and 10 minutes, both the particle size and density increased, resulting in more uniform and denser coverage (Fig. 2b and c). At a deposition time of 50 minutes (AuNPs50), pronounced agglomeration was observed (Fig. 2d), characterized by the clustering of nanoparticles due to secondary nucleation on previously formed particles.

The observed trend in nanoparticles morphology can be attributed to the dynamic interplay between competing nucleation and growth mechanisms during the deposition process. Nucleation typically initiates at high-energy surface sites, such as defects, cavities, and grain boundaries, leading to the formation of dispersed particles. As the deposition duration increases, these high-energy sites become saturated, promoting enhanced particle growth and resulting in larger and denser nanoparticles. The agglomeration observed at extended deposition durations, particularly at 50 minutes, suggests the onset secondary nucleation occurring on pre-existing particles. This phenomenon disrupts the uniform growth of particles across the substrate and marks a transition from surface-limited nucleation to particle–particle interactions.

Energy-dispersive X-ray spectroscopy (EDX) was employed to confirm the presence of gold on the fluorine-doped tin oxide (FTO) substrate. The EDX spectrum revealed characteristic peaks corresponding to gold at approximately 2–2.5 keV and 9.5–10 keV, as shown in Fig. 3. Additionally, the EDX elemental mapping confirmed the spatial distribution of Au across the

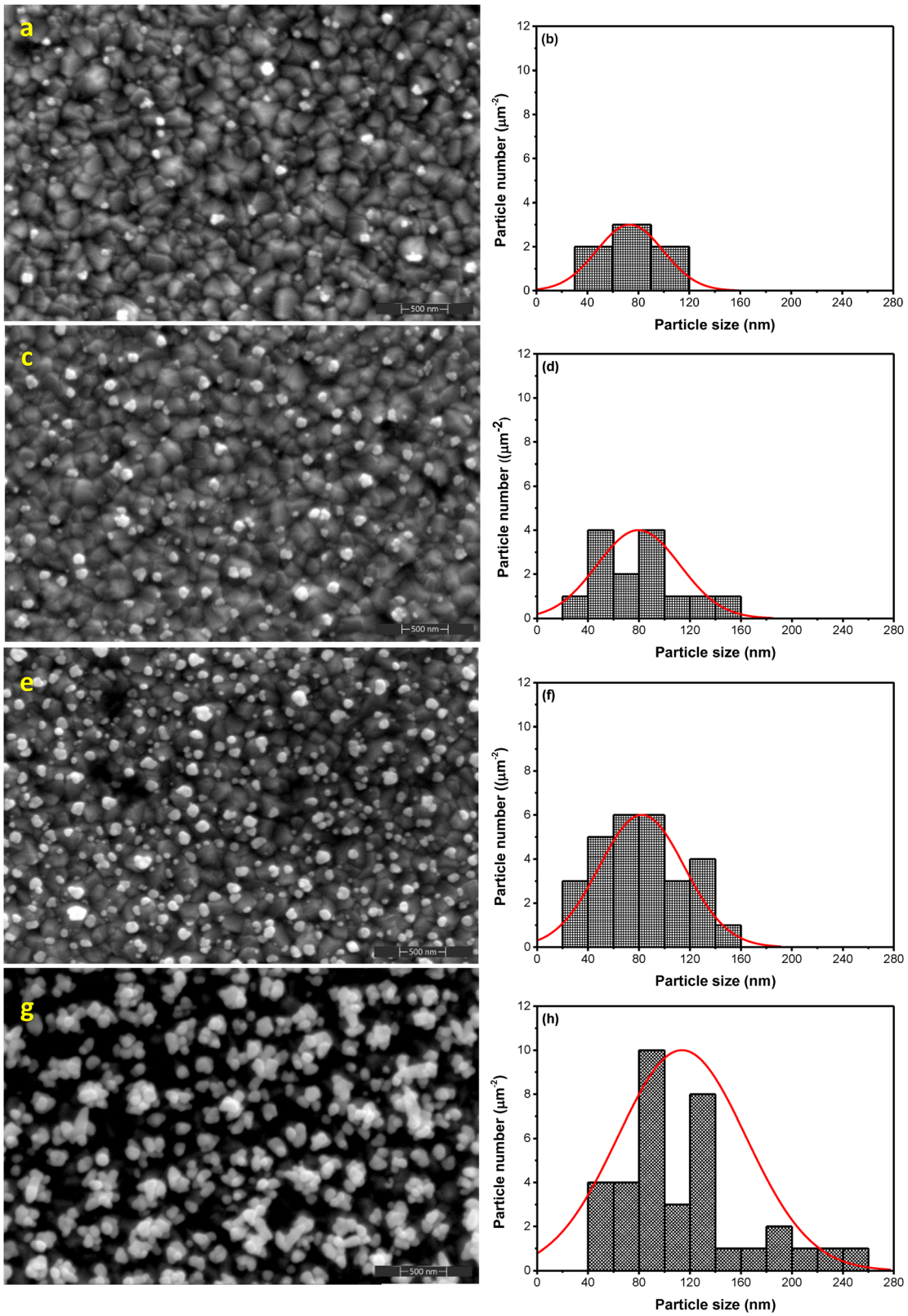

Fig. 2 FESEM micrographs and histogram of the particle size distribution of the electrodeposited AuNPs obtained with different deposition duration of 1 (a) and (b), 5 (c) and (d), 10 (e) and (f), and 50 minutes (g) and (h).

sample surface. The presence of additional peaks is attributed to the elements fluorine (F), tin (Sn), and oxygen (O) originating from the substrate. To further investigate the formation of metallic phase of Au, the samples were analyzed using X-ray

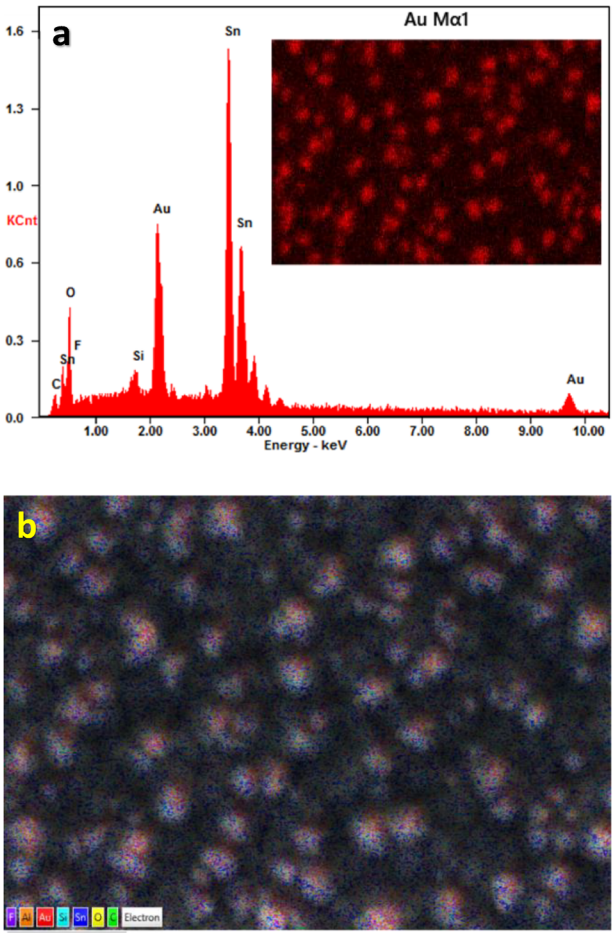

Fig. 3 A representative of EDX spectrum (a) and an EDX elemental mapping of the electrodeposited AuNPs on FTO-coated glass substrate (b). The inset is distribution of Au element over the substrate.

diffractometer (XRD). The complete XRD patterns for AuNPs deposited at 1, 5, 10, and 50 minutes are presented in Fig. S1. To better visualize the peaks associated with AuNPs, a selected region of the patterns, excluding the 2θ range from 46° to 63°, is shown in Fig. 4. From these patterns, four distinct diffraction peaks were observed at 2θ values of 38.11°, 44.36°, 64.44°, and 77.68°, corresponding to the (111), (200), (220), and (311) crystallographic planes of face-centered cubic Au, respectively. These results are consistent with standard reference data for Au (Crystallography Open Database No 96-900-8464). The (111) peak at 38.11°, although partially overlapping with the FTO substrate peak at 37.85°, became increasingly prominent with longer deposition times due to the enhanced intensity of Au diffraction. This increase in peak intensity correlates positively with extended deposition durations, which promote the growth of larger Au grains. This observation is further supported by the increase in crystallite size (Table 1), calculated from the (111) peak using the Scherrer equation. The trend aligns with the SEM micrographs (Fig. 2), indicating a positive correlation between deposition time and AuNPs particle size. These findings confirm the successful synthesis of metallic Au, where the presence of larger particles contributes to the intensified

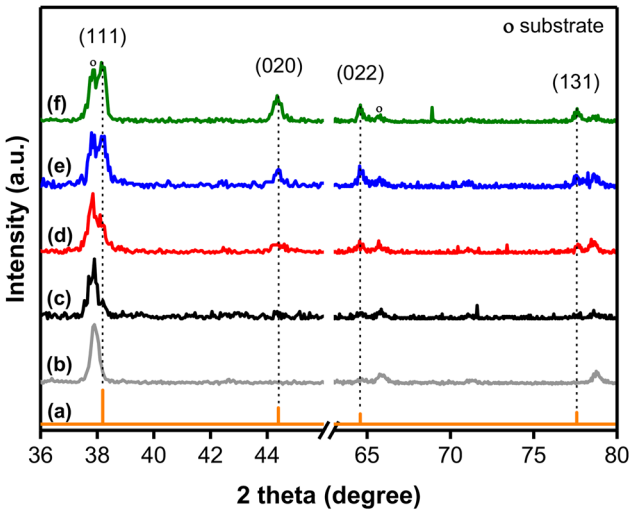

Fig. 4 XRD diffraction patterns of (b) FTO-coated glass substrate, the AUNPs electrodeposited with deposition duration of 1 (c), 5 (d), 10 (e), and 50 minutes (f), and the corresponding COD database pattern no. 96-900-8464 (a).

diffraction signals observed in samples subjected to longer deposition durations.

Nyquist plots obtained from electrochemical impedance spectroscopy (EIS) measurements (Fig. 5) demonstrate a pronounced decrease in charge transfer resistance (R_{ct}) with increasing Au deposition duration. The equivalent circuit used to fit the data is illustrated in the inset of Fig. 5a, where R_1 represents the solution resistance (R_s) and R_2 corresponds to the R_{ct}. In the Nyquist plot, the semicircular region reflects the charge transfer process, while the linear region at lower frequencies is indicative of mass transport limitations. The analysis focuses primarily on R_{ct} values, which are critical for evaluating the charge transfer kinetics of the catalytic system. Among the samples, the AuNPs1 exhibits the highest R_{ct}, attributed to the limited presence of irregularly shaped particles that provide insufficient surface area for efficient electron transfer. As the deposition duration increases, the R_{ct} progressively decreases, with AuNPs50 showing the lowest R_{ct} value, suggesting enhanced electron transfer kinetics. This reduction in R_{ct} is ascribed to the intrinsic conductivity of gold and the increased particle density grown on the FTO substrate. The greater number of deposited AuNPs significantly enlarges the electrochemically active surface area, thereby facilitating improved charge transfer and lowering the overall resistance. To further confirm this observation, the electrochemical active surface area (ECSA) was determined from the EIS data by

Table 1 Crystallite size, resistance charge transfer (R_{ct}), electrochemical active surface area (ECSA) of the AuNPs

Electrocatalyst	Crystallite size (nm)	R_{ct} (Ω)	ECSA (cm^2)
AuNPs1	21.29	25.99	3.11
AuNPs5	32.54	21.38	6.87
AuNPs10	33.04	17.69	8.30
AuNPs50	52.38	15.31	9.60

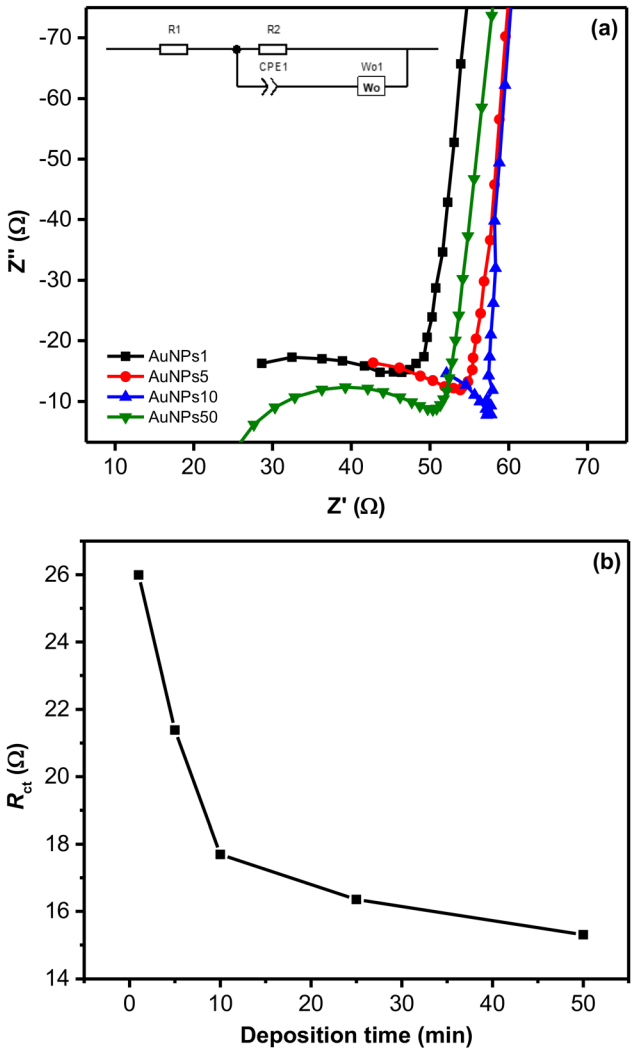

Fig. 5 Nyquist plots obtained from EIS measurements and the corresponding fitted equivalent circuit (inset) (a), along with the R_{ct} values extracted from the plots for AuNPs electrodeposited at various deposition durations (b).

evaluating the double-layer capacitance (C_{dl}) in the non-faradaic region. As shown in Table 1, ECSA values increase with longer deposition durations, indicating a greater number of active sites available for electrochemical reactions and, consequently, enhanced catalytic activity of the catalyst.

The electrocatalytic performance of AuNPs for the oxidation of ethanol was evaluated using cyclic voltammetry (CV) technique in an alkaline electrolyte comprising 0.1 M sodium hydroxide (NaOH) and 1 M ethanol. Fig. 6 presents the cyclic voltammograms of AuNPs synthesized at various deposition durations. During the anodic scan, a prominent peak at approximately 0.25 V is attributed to the oxidation of ethanol on the gold surface. In the reverse scan, a peak observed at 0.09 V corresponds to the oxidation of adsorbed carbon monoxide (CO) species, which are well-established intermediates in the ethanol oxidation pathway.[29] Control experiments conducted in NaOH electrolyte without ethanol demonstrated negligible anodic activity, confirming that the observed peaks

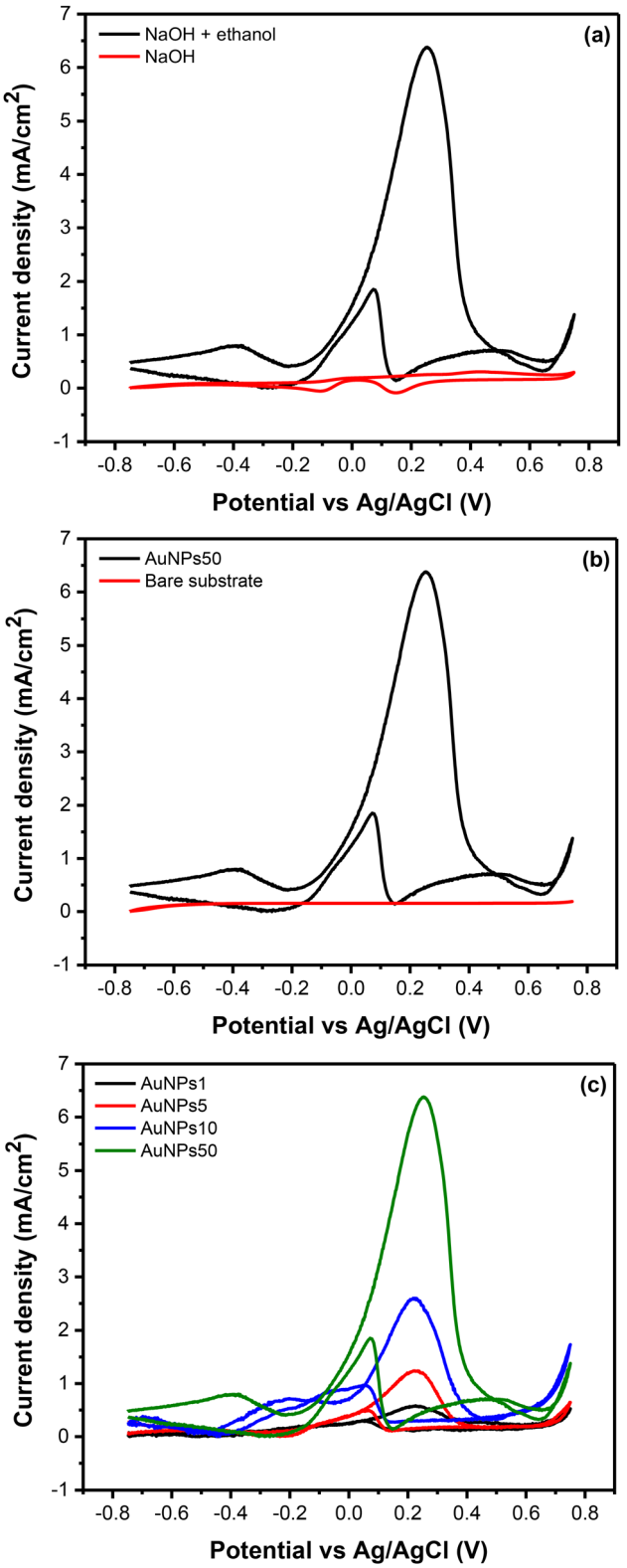

Fig. 6 Cyclic voltammograms measured using AuNPs50 in alkaline solution with and without ethanol (a), cyclic voltammograms measured using bare FTO and using AuNPs50 (b), and cyclic voltammograms measured using AuNPs prepared with different electrodeposition times.

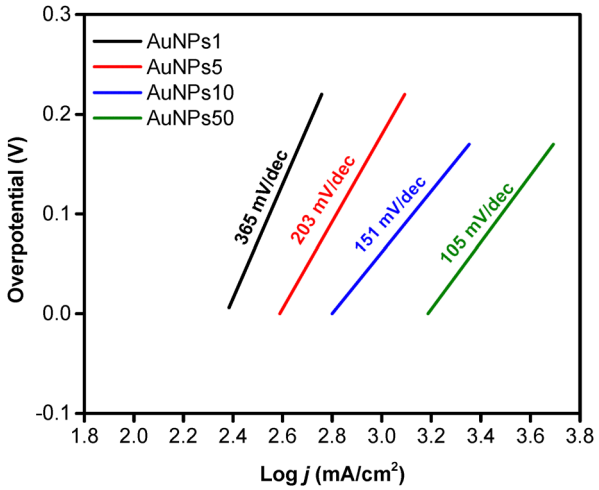

Fig. 7 Tafel slope determined of the AuNPs prepared with different electrodeposition duration.

are directly linked to the oxidation of ethanol. Additional minor peaks observed at 0.4 V, along with reductions features at −0.1 V and 0.15 V in NaOH-only system, are indicative of oxide formation and oxide stripping, respectively.[14] Furthermore, CV measurements of bare FTO substrates yielded in flat voltammograms, suggesting the absence of significant electrochemical activity. This observation further confirms the catalytic role of AuNPs in facilitating ethanol oxidation.

The catalytic activity, quantified by the anodic peak current density, exhibited a notable increase with longer deposition times, yielding values of 0.58 mA cm^{-2}, 24 mA cm^{-2}, 259 mA cm^{-2}, and 6.38 mA cm^{-2} for the samples designated as AuNPs1, AuNPs5, AuNPs10, and AuNPs50, respectively. This enhancement is attributed to the increased number of nanoparticles and improved charge transfer efficiency resulting from higher density particles achieved during extended deposition durations. The electrochemical impedance analysis supports this observation, showing a reduction in charge transfer resistance (R_{ct}) with prolonged deposition times, which facilitates more efficient electron transfer and accelerates the rate of the catalytic reaction.[30–32] Additionally, the Tafel slope (Fig. 7) values decreased from 453 mV dec^{-1} for AuNPs1 to 232 mV dec^{-1} for AuNPs50, further indicating enhanced electron transfer kinetics with prolonged deposition. As summarized in Table 2, the ratio of backward to forward current density (j_b/j_f) also declined with increasing deposition durations, suggesting enhanced catalyst stability and a greater resistance to poisoning by carbon monoxide intermediates. These results collectively demonstrate that increased particle size and density lead to improved electrocatalytic performance and long-term stability of the AuNPs.

Table 2 Onset potential (E_{onset}), maximum current density (j), cathodic to anodic ratio (j_b/j_f), and Tafel slope values of the AuNPs

Electrocatalyst	E_{onset} (V *vs.* Ag/AgCl)	j (mA cm^{-2})	j_b/j_f	Tafel slope (mV dec^{-1})
AuNPs1	−0.32	0.58	0.49	453
AuNPs5	−0.23	1.24	0.40	375
AuNPs10	−0.43	2.59	0.33	297
AuNPs50	−0.13	6.38	0.29	232

4 Conclusion

This study successfully demonstrated the synthesis of gold nanoparticles (AuNPs) on fluorine-doped tin oxide (FTO) substrates *via* square-wave pulse electrodeposition, with the deposition time identified as the key parameter influencing nanoparticle formation and performance. The results showed that increasing the deposition duration led to a more uniform nanoparticle growth, higher particle density, and improved electrocatalytic activity for ethanol oxidation in alkaline media. Among the samples, AuNPs deposited for 50 minutes demonstrated the most favorable catalytic performance, characterized by the highest current density and the lowest resistance to charge transfer. These enhancements are attributed to the increased number of active sites and electrochemical active surface area that improve charge transfer efficiency, as confirmed by electrochemical impedance spectroscopy (EIS) and cyclic voltammetry (CV) analysis. The results underscore the importance of deposition time as a tunable parameter for optimizing the catalytic performance of AuNPs. Moreover, the synthesis approach employed in this study-free from surfactants and post-treatments, highlights the potential of AuNPs as cost, effective and scalable nanocatalysts for energy-related applications.

Author contributions

Setia Budi: conceptualization, funding acquisition, methodology, supervision, visualization, writing – original draft, writing – review & editing. Annisa Auliya: writing – original draft, investigation, project administration. Hilman Syafei: investigation.

Conflicts of interest

There are no conflicts to declare.

Data availability

The data supporting this article have been included as part of the supplementary information (SI). Supplementary information is available. See DOI: **https://doi.org/10.1039/d5ma00768b**.

Acknowledgements

This research was partially funded by the National Research and Innovation Agency (BRIN) and the Lembaga Pengelola Dana Pendidikan (LPDP) under the Ministry of Finance, Republic of Indonesia, through the Riset dan Inovasi untuk Indonesia Maju (RIIM) program (grant number 1/PG.02.00.PT/LPPM/V/2025 and 110/IV/KS/11/2022).

References

1 L. M. Sousa, L. M. Vilarinho, G. H. Ribeiro, A. L. Bogado and L. R. Dinelli, *R. Soc. Open Sci.*, 2017, **4**, 170675.
2 K. Hussain and T. Hussain, *South Indian J. Biol. Sci.*, 2016, **1**, 127–133.
3 V. Borse and A. N. Konwar, *Sens. Int.*, 2020, **1**, 100051.
4 G. Zhao and G. Liu, *Nanomaterials*, 2018, **9**, 41.
5 I. A. S. Matias, A. P. C. Ribeiro, R. P. Oliveira-Silva, D. M. F. Prazeres and L. M. D. R. S. Martins, *Appl. Sci.*, 2018, **8**, 2655.
6 J. Dong, P. L. Carpinone, G. Pyrgiotakis, P. Demokritou and B. M. Moudgil, *KONA Powder Part. J.*, 2020, **37**, 224–232.
7 M. Pacaud, K. Hervé-aubert, M. Soucé, A. Abdelrahman, F. Bonnier, A. Fahmi, A. Feofanov and I. Chourpa, *Spectrochim. Acta, Part A*, 2020, **225**, 117502.
8 A. Bhattacherjee, T. Ghosh and A. Datta, *J. Exp. Nanosci.*, 2018, **13**, 50–61.
9 A. Zabihollahpoor, M. Rahimnejad, G. Najafpour and A. A. Moghadamnia, *J. Electroanal. Chem.*, 2019, **835**, 281–286.
10 S. Calamak and K. Ulubayram, *J. Mater. Sci.*, 2019, **54**, 7541–7552.
11 B. A. Varghese, R. V. R. Nair, S. Jude, K. Varma, A. Amalraj and S. Kuttappan, *J. Taiwan Inst. Chem. Eng.*, 2021, **126**, 166–172.
12 M. F. Lanjwani, M. Tuzen, M. Y. Khuhawar and T. A. Saleh, *Inorg. Chem. Commun.*, 2024, **159**, 111613.
13 Q. Zhang, T. Xia, H. Huang, J. Liu, M. Zhu, H. Yu, W. Xu, Y. Huo, C. He, S. Shen, C. Lu, R. Wang and S. Wang, *Nano Res. Energy*, 2023, **2**, e9120041.
14 A. Zhang, Y. Chen, Z. Yang, S. Ma, Y. Huang, G. Richter, P. Schützendübe, C. Zhong and Z. Wang, *ACS Appl. Energy Mater.*, 2019, **3**, 336–343.
15 S. Beyhan, K. Uosaki, J. M. Feliu and E. Herrero, *J. Electroanal. Chem.*, 2013, **707**, 89–94.
16 J. Sun, D. Wei and H. Lv, *Trans. Tianjin Univ.*, 2018, **24**, 16–24.
17 K. Raghunathan, J. Antony, S. Munir, J. P. Andreassen and S. Bandyopadhyay, *Nanoscale Adv.*, 2020, **2**, 1980–1992.
18 H. Y. Son, K. R. Kim, C. A. Hong and Y. S. Nam, *ACS Omega*, 2018, **3**, 6683–6691.
19 S. Guo, L. Wang and E. Wang, *ChemComm*, 2007, **3**, 3163–3165.
20 S. Budi, M. E. Hafizah and A. Manaf, *AIP Conf. Proc.*, 2016, **1746**, 1–7.
21 S. Budi, B. Kurniawan, D. M. Mott, S. Maenosono, A. A. Umar and A. Manaf, *Thin Solid Films*, 2017, **642**, 51–57.
22 A. Sabella, R. Syifa and N. A. Dwiyana, *Chem. Mater.*, 2022, **1**, 88–92.
23 S. Budi, M. Takahashi, M. G. Sutrisno, W. A. Adi, Z. Fairuza, B. Kurniawan, S. Maenosono and A. A. Umar, *R. Soc. Open Sci.*, 2023, **10**, 230247.
24 H. Han, J. Seo, Y. Kim, J. Lee, J. Park, S. Yoon and B. Yoo, *Electrochim. Acta*, 2024, **475**, 143694.
25 X. Zhan, J. Lian, H. Li, X. Wang, J. Zhou, K. Trieu and X. Zhang, *Electrochim. Acta*, 2021, **365**, 137391.
26 N. S. A. Malek and Y. Mohd, *Malays. J. Anal. Sci.*, 2019, **23**, 52–59.
27 S. Budi and A. Manaf, *Mater. Res. Express*, 2021, **8**, 086513.
28 S. Budi, S. Muhab, A. Purwanto, B. Kurniawan and A. Manaf, *Mater. Sci.-Pol.*, 2019, **37**, 389–394.
29 J. Feng, A. Li, Z. Lei and A. Wang, *ACS Appl. Mater. Interfaces*, 2012, **4**, 2570–2576.
30 S. Babu and P. Elumalai, *Mater. Res. Express*, 2016, **4**, 0–10.
31 B. Liu, X. Wang, S. Wang, H.-Q. Peng, T. Xiao, G. Liu, S. Bai, Y. Zhao, W. Zhang and Y.-F. Song, *Mater. Today Energy*, 2022, **28**, 101082.
32 A. S. Fazri, *Chem. Mater.*, 2023, **2**(3), 56–60.